

# Occ-BEV: Multi-Camera Unified Pre-training via 3D Scene Reconstruction

Chen Min

Peking University

minchen@stu.pku.edu.cn

**Abstract:** Multi-camera 3D perception has emerged as a prominent research field in autonomous driving, offering a viable and cost-effective alternative to LiDAR-based solutions. However, existing multi-camera algorithms primarily rely on monocular image pre-training, which overlooks the spatial and temporal correlations among different camera views. To address this limitation, we propose the first multi-camera unified pre-training framework called Occ-BEV, which involves initially reconstructing the 3D scene as the foundational stage and subsequently fine-tuning the model on downstream tasks. Specifically, a 3D decoder is designed for leveraging Bird’s Eye View (BEV) features from multi-view images to predict the 3D geometry occupancy to enable the model to capture a more comprehensive understanding of the 3D environment. One significant advantage of Occ-BEV is that it can utilize a vast amount of unlabeled image-LiDAR pairs for pre-training. The proposed multi-camera unified pre-training framework demonstrates promising results in key tasks such as multi-camera 3D object detection and semantic scene completion. When compared to monocular pre-training methods on the nuScenes dataset, Occ-BEV demonstrates a significant improvement of 2.0% in mAP and 2.0% in NDS for 3D object detection, as well as a 0.8% increase in mIOU for semantic scene completion. codes are publicly available at <https://github.com/chaytonmin/Occ-BEV>.

## 1 Introduction

The multi-camera 3D perception systems in autonomous driving offer a cost-effective solution to gather 360° environmental information around vehicles, making it a recent area of intense research [1, 2]. However, current multi-camera 3D perception models [3, 4, 5, 6] usually rely on pre-trained ImageNet models [7] or depth estimation models [3] on monocular images. These models fail to take into account the inherent spatial and temporal correlations present in multi-camera systems. Additionally, while monocular pre-training enhances the capability of image feature extraction, it does not adequately address the pre-training requirements of subsequent tasks. Autonomous driving vehicles collect vast amounts of image-LiDAR pairs, which contain valuable 3D spatial and structural information. Effectively utilizing these unlabeled image-LiDAR pairs becomes crucial for enhancing the performance of autonomous driving systems.

Recent studies, such as BEVDepth [6] and DD3D [8], have underscored the significance of depth estimation in visual-based perception algorithms. Monocular depth estimation plays a crucial role in acquiring spatial position information for objects. However, depth estimation methods typically focus on estimating the depth of object surfaces, neglecting the holistic three-dimensional structure of objects and occluded elements. For 360° multi-camera perception systems, 3D geometry occupancy grids can be employed to describe the three-dimensional scene. Achieving precise geometry occupancy prediction is instrumental in enhancing the overall 3D perception accuracy within multi-camera perception systems [9]. Hence, pre-training models for autonomous driving perception would benefit more from reconstructing the entire occupancy grids of the 3D scene, rather than solely predicting depth.

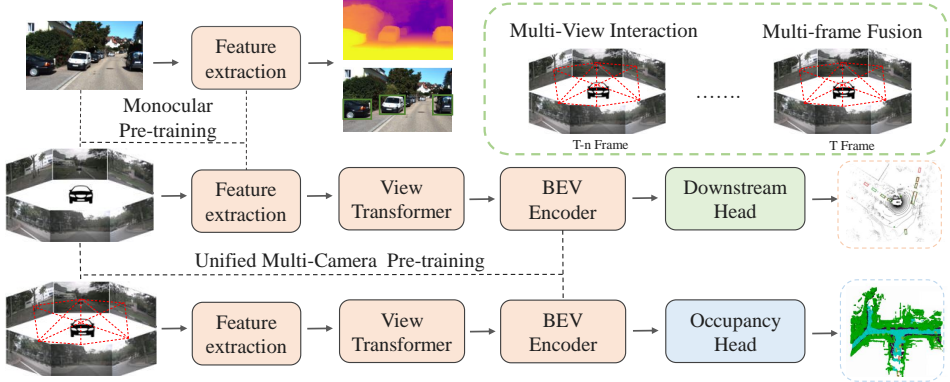


Figure 1: Comparison between monocular pre-training and our unified multi-camera pre-training. Monocular pre-training only enhances the capability of the feature extraction from a single view, whereas our proposed multi-view unified pre-training enables the incorporation of temporal and spatial information from multi-view images through 3D scene reconstruction for pre-training.

Humans possess the remarkable ability to mentally reconstruct the complete 3D geometry of occluded scenes, which is crucial for recognition and understanding. To imbue the perception system of autonomous vehicles with a similar capability, we propose a multi-camera unified pre-training method, called Occ-BEV. Our approach leverages the intuitive concept of using the multi-camera system to reconstruct the 3D scene as the foundational stage, followed by fine-tuning downstream tasks. In the case of multi-camera BEV perception, the input multi-camera images are transformed to the BEV space using advanced techniques like LSS [10] or Transformer [3], and then a geometric occupancy prediction head is incorporated to help to learn the 3D occupancy distribution, thereby enhancing the model’s understanding of the 3D surrounding scene. Due to the sparsity of single-frame point clouds, we employed multi-frame point cloud fusion as the ground truth for occupancy label generation. The decoder was solely used for pre-training purposes, while the well-trained model from pre-training was utilized to initialize the multi-camera perception models. By designing effective multi-camera unified learning methods, we enable the pre-trained model to exploit the rich spatial and temporal information inherent in the unlabeled data. This not only improves the model’s ability to understand complex 3D scenes but also reduces reliance on costly and time-consuming manual 3D annotation.

To evaluate the effectiveness of our approach, we conducted comprehensive experiments using the widely used autonomous driving dataset nuScenes [11]. The experimental results clearly demonstrate the superiority of our multi-camera unified pre-trained model compared to existing monocular pre-training methods across various 3D perception tasks, including 3D object detection and semantic scene completion. In the 3D object detection task, the proposed Occ-BEV achieves a significant improvement of 2.0% in mAP and 2.0% in NDS when compared to monocular pre-training methods. This indicates that our model is better equipped to accurately detect and localize objects in a 3D environment. For the semantic scene completion task, Occ-BEV demonstrates a noteworthy improvement of approximately 0.8% in mIOU, indicating that our model is more effective in reconstructing and predicting the semantic labels of the surrounding environment. The superior performance of our model can be attributed to its ability to effectively leverage unlabeled data, as well as its consideration of spatial and temporal correlations. By incorporating information from multiple camera views, our model can better capture the rich contextual and temporal information present in the scene, leading to enhanced perception capabilities in autonomous driving scenarios.

The main contributions of this work are listed below:

- To the best of our knowledge, we present Occ-BEV, the first multi-camera unified pre-training method that views autonomous driving perception pre-training as 3D scene reconstruction.

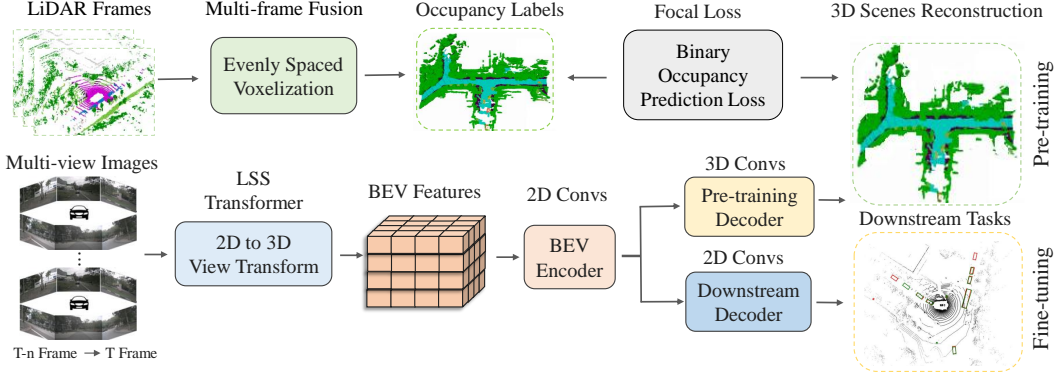


Figure 2: The overall architecture of the proposed multi-camera unified pre-training method Occ-BEV. We first transform the large-scale irregular LiDAR point clouds into volumetric representations as the geometry occupancy labels, then add an occupancy decoder with some layers of 3D convolutions to the BEV encoder. We apply binary occupancy classification as the pretext task to distinguish whether the voxel contains points. After pre-training, the lightweight decoder is discarded, and the encoder is used to warm up the backbones of downstream tasks.

- We introduce the 3D geometry occupancy prediction as the pretext task, which recovers the complete occupancy distribution of the 3D scene solely from multi-view images.
- Our multi-camera pre-training method excels in learning a unified representation, surpassing the performance of monocular pre-training in multi-view 3D object detection and semantic scene completion tasks.

## 2 Related Work

### 2.1 Multi-Camera 3D Perception

In the field of autonomous driving, vision-based 3D perception conducted in bird’s eye view (BEV) has gained significant attention in recent years. Learning-based BEV perception methods, based on 2D-to-3D view transformation, can be broadly categorized into geometry-based and Transformer-based approaches. One of the early geometry-based methods is LSS [10], which lifts each individual image into a frustum of features for each camera and then combines them into a rasterized BEV grid. Building upon LSS, BEVDet [5] introduces image-view and BEV space data augmentation techniques. BEVDepth [6] demonstrates the significance of depth and improves the quality of BEV features by incorporating explicit depth supervision from LiDAR. BEVStereo [12] and STS [13] leverage temporal multi-view stereo methods to enhance depth precision. SOLOFusion [14] and VideoBEV [15] explore long-term temporal fusion for multi-view 3D perception. DETR3D [3] is the first Transformer-based BEV method, which defines object queries in 3D space and learns from multi-view image features using a transformer decoder. Building upon DETR3D, PETR [16] enhances the approach with position embedding transformations, while BEVFormer [4] introduces temporal self-attention to fuse historical BEV features. UniAD [17] extends BEVFormer to enable multi-task learning in BEV space. Although the existing BEV perception methods have shown promising performance, they are typically initialized with ImageNet pre-trained models [7] or depth pre-trained models [8] trained on monocular images. However, there is a lack of unified pre-training methods that effectively leverage the geometry structure of multi-camera inputs.

### 2.2 Self-supervised Learning

Self-supervised Learning (SSL) has gained significant popularity in recent years as it eliminates the need for expensive data annotation. For instance, the method presented in [18] focuses on predicting the relative location of image patches as the pretext task. Another approach, as described in

[19], tackles a jigsaw puzzle prediction task, which demonstrates strong generalization capabilities for domain adaptation in object recognition. DeepCluster [20] and SwAV [21] leverage k-means clustering to obtain pseudo-labels, which are then used to train the network. Moco [22] and BYOL [23] construct contrastive views for self-supervised learning. Additionally, methods like MAE [24] and BEiT [25] employ a random patch masking approach where missing pixels or features are reconstructed using a simple autoencoder framework. In the context of automated vehicle perception, DD3D utilizes monocular depth estimation for pre-training. Voxel-MAE [26] and ALSO [27] propose predicting occupancy for LiDAR perception as the pretext task. In this work, we introduce the first multi-camera unified pre-training approach that utilizes 360° geometry occupancy prediction for vision-based perception methods.

### 3 Methodology

This section elaborates on the network architecture of Occ-BEV, as illustrated in Figure 2. First, the vision-based BEV perception methods are reviewed in Section 3.1. Then, the proposed geometry occupancy pre-training is introduced in Section 3.2, along with the comparison with existing monocular pre-training and knowledge distillation methods in Section 3.3.

#### 3.1 Review of BEV Perception

As described in related works, there are two main learning-based methods to convert 2D images to 3D space: LSS-based and Transformer-based view transformation. Our method is not limited to any specific view transformation method. In the following sections, we will provide an overview of the workflow of multi-camera perception algorithms based on the bird’s eye view.

The multi-camera input images, denoted as  $I = \{I_i, i = 1, 2, \dots, N_{view}\}$ , are initially processed by an image backbone network (e.g., ResNet-101 [28]), generating feature maps  $F_{2d} = \{F_{2d}^i\}_{i=1}^{N_{view}}$  for each camera view. These features, denoted as  $F_{2d}^i$ , are then fed into a 2D-to-3D view transformation operation to project them onto a unified bird’s-eye view representation, denoted as  $F_{bev} \in \mathbb{R}^{C \times H \times W}$ . By incorporating specific heads, diverse autonomous driving perception tasks can be accomplished on the bird’s eye view, including 3D object detection, map segmentation, object tracking, and more [17]. Current BEV perception algorithms [4, 3, 5] predominantly rely on feature extraction models (e.g., ImageNet [7]) or depth estimation models (e.g., V2-99 [8]) trained on monocular images. However, these approaches fail to consider the interplay and correlation between images captured from different camera views and frames. Consequently, there is a lack of a multi-camera unified pre-training model. In order to fully exploit the spatial and temporal relationships between different camera views, we propose a unified multi-camera pre-training model.

#### 3.2 Multi-camera Unified Pre-training

Methods such as BEVDepth [6] and DD3D [8] demonstrate the importance of depth estimation for visual-based perception algorithms. However, depth estimation can only estimate the position of the object’s surface, ignoring the occlusions of objects. For multi-camera systems, precision 3D occupancy grid prediction is beneficial to the accuracy of perception.

##### 3.2.1 Geometry Occupancy Decoder

To predict 3D geometry occupancy from BEV features  $F_{bev}$ , we initially transform the BEV features into  $F'_{bev} \in \mathbb{R}^{C' \times D \times H \times W}$ , where  $D$  represents the number of height channels, and  $C = C' \times D$ . Subsequently, we employ a 3D decoder that is specifically designed to generate 3D geometry occupancy. Our decoder comprises lightweight 3D convolution layers, with the final layer providing the probability of each voxel containing points. The decoder’s output is denoted as  $\mathbf{P} \in \mathbb{R}^{D \times H \times W \times 2}$ . During pre-training, the decoder’s primary purpose is to reconstruct occupied voxels.

### 3.2.2 Pre-training Target

Taking into account the sparse nature of single-frame LiDAR point clouds and the potential inaccuracies arising from fusing a large number of frames due to the presence of dynamic objects, we fuse the LiDAR point clouds from some keyframes as the computation source for the occupancy labels generation. In line with the standard practice in 3D perception models [29, 30, 31, 32], the LiDAR point clouds are partitioned into evenly spaced voxels. Considering the dimensions of the point clouds along  $Z \times Y \times X$  as  $D \times H \times W$  respectively, the voxel size is determined as  $v_Z \times v_H \times v_W$  correspondingly. The occupied voxels, which contain points (with a voxel value of 1), and the empty voxels (with a voxel value of 0) serve as the ground truth  $\mathbf{T} \in \mathbb{R}^{D \times H \times W \times 2}$ .

We introduce the binary geometry occupancy classification task for pre-training multi-camera perception models. The objective of this task is to train the network to accurately predict the geometry occupancy distribution of the 3D scene based on multi-view images. Taking into account the significant number of empty voxels, predicting occupancy grids poses an imbalanced binary classification problem. To accomplish this, we compute the focal loss for binary occupancy classification, utilizing the predicted occupied voxels  $\mathbf{P}$  and the ground truth occupied voxels  $\mathbf{T}$ :

$$\text{loss} = -\frac{1}{\text{batch}} \frac{1}{n} \sum_{i=1}^{\text{batch}} \sum_{j=1}^n \alpha_t \left(1 - \mathbf{P}_t^{ij}\right)^\gamma \log(\mathbf{P}_t^{ij}), \quad (1)$$

where  $\mathbf{P}^{ij}$  is the predicted probability.  $\alpha$  is set as 2 and  $\gamma$  is 0.25.  $\alpha_t = \alpha$  and  $\mathbf{P}_t^{ij} = \mathbf{P}^{ij}$  for class 1.  $\alpha_t = 1 - \alpha$  and  $\mathbf{P}_t^{ij} = 1 - \mathbf{P}^{ij}$  for class 0.  $n = D \times H \times W$  is the total number of voxels.

### 3.2.3 Pre-training for Semantic Occupancy Prediction

Recently, several algorithms such as TPVFormer [33], OpenOccupancy [34] and Occ3D [35] have extended multi-camera BEV perception to the task of surrounding semantic scene completion. However, directly predicting the 3D semantics of multi-view images requires a large amount of 3D semantic annotation for training, which can be costly and time-consuming. To address this challenge, we propose to extend our multi-camera unified pre-training algorithm to the surrounding semantic scene completion task, that is, firstly perform geometric occupancy prediction, and then fine-tune on surrounding semantic scenes completion task.

## 3.3 Comparision with Existing Methods

### 3.3.1 Comparision with Monocular Pre-training

Currently, multi-camera perception algorithms employ either monocular image pre-training on ImageNet [7] or depth estimation pre-training [8]. As shown in Figure 1, our proposed multi-camera unified pre-training model offers several advantages over monocular pre-training: (1) **Spatial-Temporal Integration**: By leveraging the spatial and temporal information from multiple camera views, the model can better comprehend the dynamic nature of the environment and make more accurate predictions. (2) **Unified Representation**: The unified pre-training approach allows the model to learn a shared representation across different camera views, promoting better knowledge transfer and reducing the need for task-specific pre-training. (3) **Perception of occluded areas**: Monocular depth estimation can only predict the surface positions of objects, while the proposed multi-camera unified pre-training method enables the overall 3D reconstruction of occluded objects.

### 3.3.2 Comparision with Knowledge Distillation

Recently, there have been advancements in knowledge distillation algorithms such as BEVDistill [36] and TiG-BEV [37], which aim to transfer knowledge from well-established 3D LiDAR detection models like CenterPoint [31] to multi-camera object detection algorithms. Similarly, our approach aims to leverage the rich spatial information present in 3D point clouds and transfer it to

Table 1: Quantitative multi-camera 3D object detection performance on the nuScenes *val* set.

Type	Method	Pre-train	Backbone	Image Size	CBGS	mAP $\uparrow$	NDS $\uparrow$	mATE $\downarrow$	mASE $\downarrow$	mAOE $\downarrow$	mAVE $\downarrow$	mAAE $\downarrow$
Transformer [3]	DETR3D [3]	FCOS3D [38]	R101-DCN	900 $\times$ 1600	✓	0.349	0.434	0.716	0.268	0.379	0.842	0.200
	DETR3D [3]	Occ-BEV	R101-DCN	900 $\times$ 1600	✓	0.360	0.461	0.701	0.260	0.372	0.730	0.188
	BEVFormer [4]	FCOS3D [38]	R101-DCN	900 $\times$ 1600	✗	0.416	0.517	0.673	0.274	0.372	0.394	0.198
	BEVFormer [4]	Occ-BEV	R101-DCN	900 $\times$ 1600	✗	0.438	0.534	0.656	0.271	0.371	0.348	0.183
LSS [10]	BEVDet [5]	ImageNet [7]	R-50	256 $\times$ 704	✗	0.286	0.372	0.724	0.278	0.590	0.873	0.247
	BEVDet [5]	Occ-BEV	R-50	256 $\times$ 704	✗	0.310	0.395	0.701	0.259	0.578	0.852	0.230
	BEVDepth [6]	ImageNet [7]	R-50	256 $\times$ 704	✗	0.351	0.475	0.639	0.267	0.479	0.428	0.198
	BEVDepth [6]	Occ-BEV	R-50	256 $\times$ 704	✗	0.376	0.492	0.620	0.259	0.466	0.425	0.187

Table 2: Quantitative multi-camera 3D object detection performance on the nuScenes test set.

Type	Method	Pre-train	Backbone	Image Size	CBGS	mAP $\uparrow$	NDS $\uparrow$	mATE $\downarrow$	mASE $\downarrow$	mAOE $\downarrow$	mAVE $\downarrow$	mAAE $\downarrow$
Transformer [3]	DETR3D [3]	DD3D [8]	v2-99	900 $\times$ 1600	✓	0.412	0.479	0.641	0.255	0.394	0.845	0.133
	DETR3D [3]	Occ-BEV	v2-99	900 $\times$ 1600	✓	0.431	0.496	0.621	0.257	0.407	0.783	0.123

multi-camera algorithms. Our unique pre-training algorithm eliminates the need for annotations or pre-trained LiDAR detection models, significantly reducing the 3D annotation requirements.

## 4 Experiments

### 4.1 Experimental Setup

We conducted extensive experiments on the nuScenes dataset [11]. For the multi-camera 3D object detection task, we adopted the training settings from the existing methods: DETR3D [3] and BEVFormer [4], which are two Transformer-based methods, and BEVDet [5] and BEVDepth [6], which is two LSS-based methods [4, 6]. The voxel size used in our approach is set as  $16 \times 200 \times 200$  for DETR3D [3] and BEVFormer [4], and  $16 \times 128 \times 128$  for BEVDet and BEVDepth. We performed pre-training for a total of 24 epochs using the training set of the nuScenes dataset. The occupancy decoder in our model consists of two layers of 3D convolutional layers. For more detailed information about the parameter setups, please refer to the papers on DETR3D [3], BEVFormer [4], BEVDet [5] and BEVDepth [6]. All experiments were conducted using 8 A40 GPU cards.

### 4.2 Results on Downstream Tasks

#### 4.2.1 Multi-Camera 3D Object Detection

We first conducted an evaluation of Occ-BEV on the validation set of nuScenes. As shown in Table 1, our multi-camera unified pre-training method exhibited significant improvements over monocular FCOS3D [38]. It surpassed DETR3D [3] by achieving a 3.0% increase in NDS and 1.0% in mAP. Additionally, it outperformed BEVFormer [4] with a 1.5% improvement in NDS and 2.0% in mAP. We present the convergence curve of BEVFormer [4] in Figure 3. Our unified pre-training significantly enhances BEVFormer [4] at epoch two, achieving a 4% increase in NDS. This demonstrates that our unified pre-training method delivers accurate object position information from a global perspective. Similarly, for the LSS-based methods and BEVDepth [6], initialized with monocular pre-training on ImageNet [7], our multi-camera unified pre-training method showed an improvement of approximately 2.0% in NDS and 2.5% in mAP.

We conducted additional experiments on the nuScenes test set to validate the effectiveness of our proposed multi-camera unified pre-training method via 3D scene reconstruction compared to pre-training based on monocular depth estimation. As presented in Table 2, our multi-camera unified pre-training method demonstrated a significant improvement of 2% in both mAP and NDS compared to the DETR3D [3] model pre-trained on DD3D [8] for depth estimation. This highlights the effectiveness and superiority of our pre-training approach in enhancing the performance of 3D perception tasks. Compared to the monocular depth estimation approach of DD3D [8], our pre-training method considers the complete 3D structure of objects, beyond the partial surfaces captured by LiDAR. Moreover, it incorporates the learning of multi-view and temporal information, allowing for

Table 3: Quantitative segmentation performance on the 3D occupancy prediction challenge [39].

Methods	Pre-train	mIoU↑	others	barrier	bicycle	bus	car	construction	motorcycle	pedestrian	traffic-cone	trailer	truck	driveable	others	sidewalk	terrain	manmade	vegetation
BEVFormer [4]	FCOS3D [38]	23.70	10.24	36.77	11.70	29.87	38.92	10.29	22.05	16.21	14.69	27.44	23.13	48.19	33.10	29.80	17.64	19.01	13.75
BEVStereo [12]	BEVDet4D [5]	42.78	22.45	47.95	28.13	40.29	53.79	27.60	35.18	29.64	31.69	45.49	37.71	81.88	49.16	55.03	51.00	50.87	39.46
BEVStereo [12]	Occ-BEV	43.55	24.00	49.84	30.02	41.10	54.13	26.95	36.60	29.40	30.98	47.99	38.48	82.24	48.96	56.05	49.95	52.37	41.26

a more comprehensive understanding of the scene. The above results indicated that our proposed Occ-BEV model has a promising application in autonomous driving field.

We also compared our proposed multi-camera unified pre-training method with the knowledge distillation approach BEVDistill [36]. As shown in Table 5, our method demonstrates comparable performance to the distillation method trained on annotated LiDAR point clouds data. It is worth noting that our approach offers higher efficiency and broader applicability since it does not rely on data annotation or training of LiDAR point clouds models as BEVDistill [36].

#### 4.2.2 Multi-Camera Semantic Occupancy Prediction

We also evaluated the performance of our proposed multi-camera unified pre-training method on the task of multi-camera semantic scene completion. Compared to BEV perception, the task of predicting semantic labels for each voxel in 3D space, known as multi-camera semantic scene completion, is more challenging. To tackle this challenge, we decomposed the task into two steps: first reconstructing the 3D scene as the fundamental model and then simultaneously reconstructing and predicting semantics. As shown in Table 3, on the Occ-3D [35] test set, our algorithm achieved a 0.8% improvement in mIoU compared to BEVDet4D [40], highlighting the effectiveness of our approach in addressing the complexities of multi-camera semantic occupancy grid prediction.

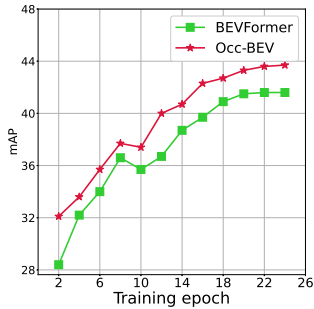


Figure 3: Performance curves.

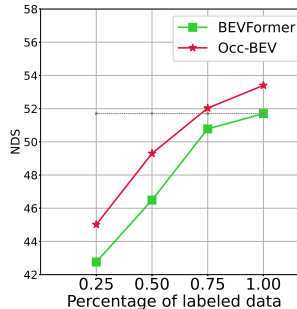


Figure 4: Label-efficiency.

Frames	mAP↑	NDS↑	mATE↓
0	0.416	0.517	0.673
1	0.417	0.523	0.661
3	0.438	0.534	0.656
5	0.429	0.525	0.659

Table 4: Impacts of multi-frame fusion. The occupancy labels were obtained by merging LiDAR point clouds from the current frame, preceding keyframes, succeeding keyframes, and their corresponding non-keyframes.

Methods	mAP↑	NDS↑
BEVFormer [4]	0.352	0.423
BEVDistill [36]	0.386	0.457
Occ-BEV	0.389	0.459

Table 5: Comparison with BEVDistill [36].

Methods	mAP↑	NDS↑	mATE↓
BEVFormer [4]	0.416	0.517	0.673
Occ-BEV	0.438	0.534	0.656
Supervision	0.445	0.544	0.648

Table 6: Explicit semantic occupancy supervision.

### 4.3 Ablation Studies

In this section, we perform thorough ablation experiments with BEVFormer [4] on nuScenes *val* set.

#### 4.3.1 Data-efficient Learner

Fine-tuning models using limited labelled data is made possible through pre-training. In order to evaluate the data efficiency of Occ-BEV, we conducted experiments using varying amounts of la-

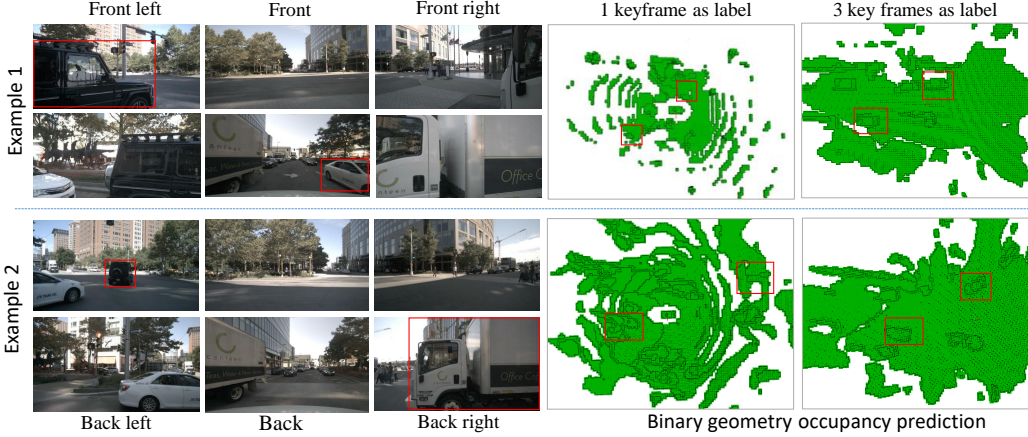


Figure 5: Visualization of 3D scene reconstruction.

labelled data for fine-tuning. BEVFormer [4] was utilized as the backbone and assessed the detection performance of the model on the nuScenes validation set. The results, as depicted in Figure 4, demonstrate that when Occ-BEV is trained with 75% of the labelled data, it achieves the same performance as BEVFormer trained on the complete dataset. Moreover, even with only 25% of the samples available for fine-tuning, our Occ-BEV model outperforms BEVFormer by 1% in mAP, highlighting its remarkable data efficiency and its potential to reduce the reliance on expensive human-annotated 3D data.

#### 4.3.2 Multi-frame Fusion

We conducted an analysis of the influence of the number of fused LiDAR frames on the pre-trained model. As more frames were fused, the density of the point clouds increased. Our comparison included single-frame fusion, 3-frame fusion and 5-frame fusion (including the corresponding non-key frames) and the results are presented in Table 4. It is clear that the model’s accuracy initially improved with an increasing number of fused point clouds but started to decline afterwards. This finding suggests that fusing multiple frames of point clouds can enhance the effectiveness of the pre-trained model. However, it is important to note that excessive fusion of frames introduces uncertainty due to the presence of dynamic objects. This uncertainty can lead to errors in the fusion process and subsequently lower the accuracy of the model.

#### 4.3.3 Explicit Supervision

Labeled 3D data can be utilized to handle dynamic objects separately during the point cloud fusion process, resulting in more precise occupancy grid ground truth for multi-frame fusion. Subsequently, we examined the impact of explicit occupancy grid prediction on the model’s performance. The results in Table 6 demonstrate that incorporating explicit supervision leads to a notable improvement of 3% in mAP and NDS compared to BEVFormer [4]. Furthermore, when compared to unlabeled multi-frame fused point cloud pre-training, there is a 1% increase in mAP. These findings highlight the potential of leveraging labelled data for explicit occupancy grid prediction supervision. Moreover, they further support the proposition that occupancy grid prediction enables the model to learn the data distribution of the entire 3D scene, thereby enhancing the accuracy of downstream tasks.

#### 4.4 Qualitative Evaluation

As shown in Figure 5, we present several reconstructed 3D scenes. It can be observed that using single-frame point clouds as the supervision for occupancy grid generation results in incomplete reconstructions due to the sparse nature of the point clouds. On the other hand, using three keyframes and their corresponding non-key frames (approximately 20 frames in total) as the supervision in-

formation allows for more complete reconstructions of static scenes. Furthermore, dynamic objects such as vehicles can also be accurately reconstructed.

**Limitations.** Although our multi-camera unified pre-training approach has demonstrated promising results, there are several limitations to consider: (1) The 3D convolutions in the decoder limits its applicability to tasks requiring high-resolution occupancy reconstruction. We will explore the cascade refine strategy. (2) Currently, we rely on LiDAR to obtain ground truth occupancy grids. In the future, we will explore the use of NeRF [41, 42, 43, 44] and MVS [45, 46, 47, 48] algorithms to reconstruct 3D scenes solely from images and obtain ground truth data. (3) Dynamic targets can lead to inaccurate ground truth, which can be addressed with dynamic object detection algorithms.

## 5 Conclusion

We defined the task of multi-camera unified pre-training and proposed the first unified pre-training algorithm that has demonstrated exceptional performance on various autonomous driving tasks, such as multi-camera 3D object detection and surrounding semantic scene completion. Pre-training via 3D scene reconstruction offers promising opportunities for enhanced unified representation learning and decreased reliance on annotated 3D data. Future work should focus on addressing the limitations mentioned and further improving the performance and applicability of our approach in real-world autonomous driving scenarios.

## References

- [1] Y. Ma, T. Wang, X. Bai, H. Yang, Y. Hou, Y. Wang, Y. Qiao, R. Yang, D. Manocha, and X. Zhu. Vision-centric bev perception: A survey. *arXiv preprint arXiv:2208.02797*, 2022.
- [2] H. Li, C. Sima, J. Dai, W. Wang, L. Lu, H. Wang, E. Xie, Z. Li, H. Deng, H. Tian, et al. Delving into the devils of bird’s-eye-view perception: A review, evaluation and recipe. *arXiv preprint arXiv:2209.05324*, 2022.
- [3] Y. Wang, V. C. Guizilini, T. Zhang, Y. Wang, H. Zhao, and J. Solomon. Detr3d: 3d object detection from multi-view images via 3d-to-2d queries. In *Conference on Robot Learning*, pages 180–191. PMLR, 2022.
- [4] Z. Li, W. Wang, H. Li, E. Xie, C. Sima, T. Lu, Q. Yu, and J. Dai. Bevformer: Learning bird’s-eye-view representation from multi-camera images via spatiotemporal transformers. *arXiv preprint arXiv:2203.17270*, 2022.
- [5] J. Huang, G. Huang, Z. Zhu, and D. Du. Bevdet: High-performance multi-camera 3d object detection in bird-eye-view. *arXiv preprint arXiv:2112.11790*, 2021.
- [6] Y. Li, Z. Ge, G. Yu, J. Yang, Z. Wang, Y. Shi, J. Sun, and Z. Li. Bevdepth: Acquisition of reliable depth for multi-view 3d object detection. *arXiv preprint arXiv:2206.10092*, 2022.
- [7] J. Deng, W. Dong, R. Socher, L.-J. Li, K. Li, and L. Fei-Fei. Imagenet: A large-scale hierarchical image database. In *2009 IEEE conference on computer vision and pattern recognition*, pages 248–255. Ieee, 2009.
- [8] D. Park, R. Ambrus, V. Guizilini, J. Li, and A. Gaidon. Is pseudo-lidar needed for monocular 3d object detection? In *Proceedings of the IEEE/CVF International Conference on Computer Vision*, pages 3142–3152, 2021.
- [9] Y. Shi, K. Jiang, J. Li, J. Wen, Z. Qian, M. Yang, K. Wang, and D. Yang. Grid-centric traffic scenario perception for autonomous driving: A comprehensive review. *arXiv preprint arXiv:2303.01212*, 2023.

[10] J. Phlion and S. Fidler. Lift, splat, shoot: Encoding images from arbitrary camera rigs by implicitly unprojecting to 3d. In *European Conference on Computer Vision*, pages 194–210. Springer, 2020.

[11] H. Caesar, V. Bankiti, A. H. Lang, S. Vora, V. E. Liong, Q. Xu, A. Krishnan, Y. Pan, G. Baldan, and O. Beijbom. nuscenes: A multimodal dataset for autonomous driving. In *Proceedings of the IEEE/CVF conference on computer vision and pattern recognition*, pages 11621–11631, 2020.

[12] Y. Li, H. Bao, Z. Ge, J. Yang, J. Sun, and Z. Li. Bevstereo: Enhancing depth estimation in multi-view 3d object detection with dynamic temporal stereo. *arXiv preprint arXiv:2209.10248*, 2022.

[13] Z. Wang, C. Min, Z. Ge, Y. Li, Z. Li, H. Yang, and D. Huang. Sts: Surround-view temporal stereo for multi-view 3d detection. *arXiv preprint arXiv:2208.10145*, 2022.

[14] J. Park, C. Xu, S. Yang, K. Keutzer, K. Kitani, M. Tomizuka, and W. Zhan. Time will tell: New outlooks and a baseline for temporal multi-view 3d object detection. *arXiv preprint arXiv:2210.02443*, 2022.

[15] C. Han, J. Sun, Z. Ge, J. Yang, R. Dong, H. Zhou, W. Mao, Y. Peng, and X. Zhang. Exploring recurrent long-term temporal fusion for multi-view 3d perception. *arXiv preprint arXiv:2303.05970*, 2023.

[16] Y. Liu, T. Wang, X. Zhang, and J. Sun. Petr: Position embedding transformation for multi-view 3d object detection. *arXiv preprint arXiv:2203.05625*, 2022.

[17] Y. Hu, J. Yang, L. Chen, K. Li, C. Sima, X. Zhu, S. Chai, S. Du, T. Lin, W. Wang, L. Lu, X. Jia, Q. Liu, J. Dai, Y. Qiao, and H. Li. Planning-oriented autonomous driving. In *Proceedings of the IEEE/CVF Conference on Computer Vision and Pattern Recognition*, 2023.

[18] C. Doersch, A. Gupta, and A. A. Efros. Unsupervised visual representation learning by context prediction. In *Proceedings of the IEEE international conference on computer vision*, pages 1422–1430, 2015.

[19] F. M. Carlucci, A. D’Innocente, S. Bucci, B. Caputo, and T. Tommasi. Domain generalization by solving jigsaw puzzles. In *Proceedings of the IEEE/CVF Conference on Computer Vision and Pattern Recognition*, pages 2229–2238, 2019.

[20] M. Caron, P. Bojanowski, A. Joulin, and M. Douze. Deep clustering for unsupervised learning of visual features. In *Proceedings of the European conference on computer vision (ECCV)*, pages 132–149, 2018.

[21] M. Caron, I. Misra, J. Mairal, P. Goyal, P. Bojanowski, and A. Joulin. Unsupervised learning of visual features by contrasting cluster assignments. *Advances in Neural Information Processing Systems*, 33:9912–9924, 2020.

[22] K. He, H. Fan, Y. Wu, S. Xie, and R. Girshick. Momentum contrast for unsupervised visual representation learning. In *Proceedings of the IEEE/CVF conference on computer vision and pattern recognition*, pages 9729–9738, 2020.

[23] J.-B. Grill, F. Strub, F. Altché, C. Tallec, P. Richemond, E. Buchatskaya, C. Doersch, B. Avila Pires, Z. Guo, M. Gheshlaghi Azar, et al. Bootstrap your own latent-a new approach to self-supervised learning. *Advances in neural information processing systems*, 33:21271–21284, 2020.

[24] K. He, X. Chen, S. Xie, Y. Li, P. Dollár, and R. Girshick. Masked autoencoders are scalable vision learners. In *Proceedings of the IEEE/CVF Conference on Computer Vision and Pattern Recognition*, pages 16000–16009, 2022.

[25] H. Bao, L. Dong, S. Piao, and F. Wei. Beit: Bert pre-training of image transformers. *arXiv preprint arXiv:2106.08254*, 2021.

[26] C. Min, D. Zhao, L. Xiao, Y. Nie, and B. Dai. Voxel-mae: Masked autoencoders for pre-training large-scale point clouds. *arXiv preprint arXiv:2206.09900*, 2022.

[27] A. Boulch, C. Sautier, B. Michele, G. Puy, and R. Marlet. Also: Automotive lidar self-supervision by occupancy estimation. *arXiv preprint arXiv:2212.05867*, 2022.

[28] K. He, X. Zhang, S. Ren, and J. Sun. Deep residual learning for image recognition. In *Proceedings of the IEEE conference on computer vision and pattern recognition*, pages 770–778, 2016.

[29] Y. Yan, Y. Mao, and B. Li. Second: Sparsely embedded convolutional detection. *Sensors*, 18(10):3337, 2018.

[30] S. Shi, C. Guo, L. Jiang, Z. Wang, J. Shi, X. Wang, and H. Li. Pv-rcnn: Point-voxel feature set abstraction for 3d object detection. In *Proceedings of the IEEE/CVF Conference on Computer Vision and Pattern Recognition*, pages 10529–10538, 2020.

[31] T. Yin, X. Zhou, and P. Krahenbuhl. Center-based 3d object detection and tracking. In *Proceedings of the IEEE/CVF conference on computer vision and pattern recognition*, pages 11784–11793, 2021.

[32] X. Zhu, H. Zhou, T. Wang, F. Hong, Y. Ma, W. Li, H. Li, and D. Lin. Cylindrical and asymmetrical 3d convolution networks for lidar segmentation. In *Proceedings of the IEEE/CVF conference on computer vision and pattern recognition*, pages 9939–9948, 2021.

[33] Y. Huang, W. Zheng, Y. Zhang, J. Zhou, and J. Lu. Tri-perspective view for vision-based 3d semantic occupancy prediction. *arXiv preprint arXiv:2302.07817*, 2023.

[34] X. Wang, Z. Zhu, W. Xu, Y. Zhang, Y. Wei, X. Chi, Y. Ye, D. Du, J. Lu, and X. Wang. Openoccupancy: A large scale benchmark for surrounding semantic occupancy perception. *arXiv preprint arXiv:2303.03991*, 2023.

[35] X. Tian, T. Jiang, L. Yun, Y. Wang, Y. Wang, and H. Zhao. Occ3d: A large-scale 3d occupancy prediction benchmark for autonomous driving. *arXiv preprint arXiv:2304.14365*, 2023.

[36] Z. Chen, Z. Li, S. Zhang, L. Fang, Q. Jiang, and F. Zhao. Bevdistill: Cross-modal bev distillation for multi-view 3d object detection. *arXiv preprint arXiv:2211.09386*, 2022.

[37] P. Huang, L. Liu, R. Zhang, S. Zhang, X. Xu, B. Wang, and G. Liu. Tig-bev: Multi-view bev 3d object detection via target inner-geometry learning. *arXiv preprint arXiv:2212.13979*, 2022.

[38] T. Wang, X. Zhu, J. Pang, and D. Lin. FCOS3D: Fully convolutional one-stage monocular 3d object detection. In *Proceedings of the IEEE/CVF International Conference on Computer Vision (ICCV) Workshops*, 2021.

[39] Cvpr 2023 occupancy prediction challenge, 2023. URL <https://github.com/CVPR2023-3D-Occupancy-Prediction/CVPR2023-3D-Occupancy-Prediction>.

[40] J. Huang and G. Huang. Bevdet4d: Exploit temporal cues in multi-camera 3d object detection. *arXiv preprint arXiv:2203.17054*, 2022.

[41] B. Mildenhall, P. P. Srinivasan, M. Tancik, J. T. Barron, R. Ramamoorthi, and R. Ng. Nerf: Representing scenes as neural radiance fields for view synthesis. *Communications of the ACM*, 65(1):99–106, 2021.

- [42] J. T. Barron, B. Mildenhall, M. Tancik, P. Hedman, R. Martin-Brualla, and P. P. Srinivasan. Mip-nerf: A multiscale representation for anti-aliasing neural radiance fields. In *Proceedings of the IEEE/CVF International Conference on Computer Vision*, pages 5855–5864, 2021.
- [43] M. Tancik, V. Casser, X. Yan, S. Pradhan, B. Mildenhall, P. P. Srinivasan, J. T. Barron, and H. Kretzschmar. Block-nerf: Scalable large scene neural view synthesis. In *Proceedings of the IEEE/CVF Conference on Computer Vision and Pattern Recognition*, pages 8248–8258, 2022.
- [44] A. Pumarola, E. Corona, G. Pons-Moll, and F. Moreno-Noguer. D-nerf: Neural radiance fields for dynamic scenes. In *Proceedings of the IEEE/CVF Conference on Computer Vision and Pattern Recognition*, pages 10318–10327, 2021.
- [45] Q. Zhu, C. Min, Z. Wei, Y. Chen, and G. Wang. Deep learning for multi-view stereo via plane sweep: A survey. *arXiv preprint arXiv:2106.15328*, 2021.
- [46] Y. Yao, Z. Luo, S. Li, T. Fang, and L. Quan. Mvsnet: Depth inference for unstructured multi-view stereo. In *Proceedings of the European conference on computer vision (ECCV)*, pages 767–783, 2018.
- [47] Z. Wei, Q. Zhu, C. Min, Y. Chen, and G. Wang. Aa-rmvsnet: Adaptive aggregation recurrent multi-view stereo network. In *Proceedings of the IEEE/CVF International Conference on Computer Vision*, pages 6187–6196, 2021.
- [48] Z. Wei, Q. Zhu, C. Min, Y. Chen, and G. Wang. Bidirectional hybrid lstm based recurrent neural network for multi-view stereo. *IEEE Transactions on Visualization and Computer Graphics*, 2022.